McMASTER UNIVERSITY

HAMILTON, ONTARIO, CANADA

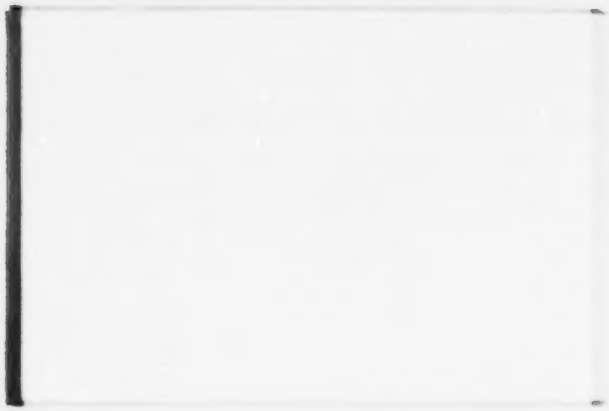

DEPARTMENT OF MATERIALS SCIENCE & ENGINEERING

CONTRACT SERIAL NO. OST 85-00261
REQUISITION NUMBER 23440-5-9171
CONTRACTOR: McMaster University

THE OPTIMIZATION OF INJECTION TECHNOLOGY FOR HIGH QUALITY STEEL

PHASE II - FINAL REPORT

CALCIUM TREATMENT OF STEEL

by

G.A. IRONS, W.-K. LU and D.-Z. LU

Department of Materials Science and Engineering

McMaster University

Hamilton, Ontario

L8S 4L7

March 31, 1988

MICROMEDIA

53 pp

This Final Report is respectfully submitted to Supply and Services Canada and the Physical Metallurgy Research Laboratory of the Ministry of Energy, Mines and Resources under the terms of the Contract "The Optimization of Injection Technology for High Quality Steel-Phase II", 20ST.23440-5-9171.

Dr. G.A. Irons
Principal Investigator
Associate Professor

Dr. W.-K. Lu
Co-Principal Investigator
Stelco Professor

Department of Materials Science and Engineering
McMaster University
Hamilton, Ontario
L8S 4L7

March 31, 1988

TABLE OF CONTENTS

LIST OF TABLES 4

LIST OF FIGURES 5

ACKNOWLEDGMENTS 7

SUMMARY AND CONCLUSIONS 8

1.0 INTRODUCTION 9

2.0 EXPERIMENTAL 10
- 2.1 APPARATUS 10
  - 2.1.1 Furnace System 10
  - 2.1.2 Oxygen Measurements in the Furnace Atmosphere 10
  - 2.1.3 Oxygen Activity in Molten Steel 10
- 2.2 MATERIALS 11
- 2.3 CHEMICAL ANALYSIS 11
  - 2.3.1 Total Aluminum and Calcium 11
  - 2.3.2 Acid Soluble Aluminum (ASA) 11
  - 2.3.3 Total Sulphur and Oxygen 11
- 2.4 INCLUSION ANALYSIS 12
- 2.5 EXPERIMENTAL DESIGN 12
- 2.6 PROCEDURE 12

3.0 RESULTS 14
- 3.1 BULK CHEMICAL RESULTS 14
- 3.2 INCLUSION DISTRIBUTION AND CHEMICAL ANALYSIS 14
  - 3.2.1 Area Fraction of Inclusions 14
  - 3.2.2 Chemical Analysis of Inclusions 16
  - 3.2.3 Comparison between Bulk Chemical and Inclusion Analysis 17
- 3.3 CALCIUM PICK-UP RATES 18
- 3.4 CALCIUM FADING RATES 19
- 3.5 DESULPHURIZATION AND DEOXIDATION RATES 19

4.0 DISCUSSION 20
- 4.1 CALCIUM RECOVERY 20
- 4.2 REACTION MECHANISM 20
- 4.3 COMPARISONS WITH FULL-SCALE PROCESSES 21

5.0 WORKSHOP ON CALCIUM TREATMENT OF STEEL 22

6.0 REFERENCES 23

7.0 FIGURES 24

LIST OF TABLES

Table I: Experimental Design of Calcium Wire Injection

Table II: Summary of Experimental Conditions

Table III: Designation of Inclusion Classifications

Table IV: Comparison of Bulk and Inclusion Chemical Analysis

Table V: Comparison with Full-Scale Injection Processes

LIST OF FIGURES

Figure 1: Schematic view of the vacuum furnace facility showing the injection of wire into the melt.

Figure 2: Comparison of oxygen activities calculated from purely ionic conduction, electronic plus ionic conduction and the correlation developed by CRM and Electro-Nite.

Figure 3: The changes of total calcium, oxygen activity, a_o, total oxygen, sulphur content, acid soluble aluminum and total aluminum content for an injection without any synthetic slag addition (H3R1).

Figure 4: The changes of total calcium, oxygen activity, a_o, total oxygen, sulphur content, acid soluble aluminum and total aluminum content for an injection with a synthetic slag addition (H6R1).

Figure 5: The CaS-MnS phase diagram.

Figure 6: The Al_2O_3-CaO phase diagram.

Figure 7A: SEM micrograph of a sulphide inclusion.

Figure 7B: SEM micrograph of an oxide inclusion.

Figure 8: The size distribution for the inclusions from injection H6R1.

Figure 9: The percentage area (compared to scanned area) of each inclusion type as a function of the total bulk calcium content of the steel for injection H6R1.

Figure 10: The effect of sulphur content on the area of the inclusion types during injection H6R1.

Figure 11: The effect of the acid soluble aluminum content on the area of each inclusion type.

Figure 12: The area of each inclusion type during and after injection H6R1.

Figure 13: The total area of all inclusions as a percent of the scanned area during injection H6R1.

Figure 14: The calcium content of the Ca(Mn)S inclusions as a function of the total calcium content of the steel during injection H6R1.

Figure 15: The calcium content of the Ca(Mn)S inclusions as a function of the acid soluble aluminum content of the steel for three different injections.

Figure 16: The calcium content of the calcium aluminate inclusions, CA_x, during injection H6R1. The total calcium content of the steel is also shown for the same samples.

Figure 17: The calcium content of the calcium aluminate inclusions, CA_x, as a function of the calcium content of the steel. The data obtained by Hilty and Farrell [9] are also shown.

Figure 18: The effect of the acid soluble aluminum content on the calcium content of the calcium aluminate inclusions, CA_x, for three different injections with the same total calcium and sulphur content in the steel.

Figure 19: The effect of the sulphur content of the steel on the calcium content of the calcium aluminates, CA_x, for three different injections with the same total calcium and acid soluble aluminum content in the steel.

Figure 20: The effect of the oxygen activity measured by the oxygen probe and the sulphur content of the steel.

Figure 21: The effect of the calcium wire feeding rate on the rate of total calcium content pick-up in the steel for three different injections with the same initial sulphur content, 0.017 and acid soluble aluminum content, 0.01%.

Figure 22: The apparent rate constants for calcium pick-up, K_{DIS}, and calcium fading, K_{EVP}, as a function of the calcium feed rate. The equations represent multiple regressions on the feed rate, melt temperature and melt depth, indicating that the feed rate is the most significant variable.

Figure 23: The logarithm of the total calcium content as a function of time after the end of calcium feeding.

Figure 24: The effect of calcium feed rate on the desulphurization (TOP) and changes in oxygen activity (BOTTOM).

Figure 25: The effect of the acid soluble aluminum content of the steel on the changes in sulphur content (TOP) and oxygen activity (BOTTOM).

Figure 26: The apparent first order rate constant for desulphurization, K_S as a function of calcium feed rate. The data is very similar to the rate constant for calcium pick-up, K_{DIS}. The equations represent regressions on the most important variables, the feed rate, X, and the temperature, T.

Figure 27: The calcium recovery as a function of time for three different injection rates.

Figure 28: A schematic representation of the proposed model to explain the present experimental results.

ACKNOWLEDGMENTS

The authors would like to acknowledge the assistance of Mr. O. Kelly and Dr. L.-K. Chiang with the experimental work. Mr. M. Van Oosten provided his expertise and assistance with the chemical analysis.

Thanks also go to Stelco, Inc. personnel for assistance in several areas: to Mr. D. McCutcheon for supplying the steel for the experiments and arranging the quantitative SEM analysis, to Mr. S. Koprick for performing the SEM analysis, and to Dr. O. Bhargava for arranging the acid soluble aluminum analysis.

Finally, the financial support of the Physical Metallurgy Research Laboratories (PMRL) of CANMET are gratefully acknowledged, as well as the useful discussions with Dr. A.R. Palmer who monitored this project.

SUMMARY AND CONCLUSIONS

1. A facility for the injection of calcium wire into 40 kg heats of steel has been developed. The wire can be fed in under controlled atmosphere and dip samples, and temperature and oxygen probe measurements taken during and after injection. Analytical procedures for total calcium and aluminum have also been developed. This facility is available to Canadian Industry for further work. A Workshop was held on February 29, 1988 to present these results to Canadian Industry.

2. Fourteen, well-controlled injections of calcium into AISI 1045 were performed. The major operational variables were the acid soluble aluminum content, the sulphur content and the calcium feed rate.

3. During injection there was an initial rapid rise of total calcium content rising to a steady-state level. Both the pick-up rate and the steady-state level increased with calcium feed rate. After injection the total calcium content decreased rapidly, apparently following first-order kinetics.

4. The rate of desulphurization and deoxidation both increase with the calcium feed rate. Desulphurization proceeds to lower levels as the acid soluble aluminum content increases.

5. Analysis of inclusions obtained during calcium injection indicates that large amounts of CaO and CaS are formed, and that most of the bulk total calcium content is calcium contained as inclusions.

6. The oxygen activity in the melt was apparently controlled by the equilibrium between CaO, CaS and the sulphur content of the melt.

7. MnS sulphide inclusions tended to be transformed to calcium-rich inclusions with increased calcium treatment, increased acid soluble aluminum and decreased oxygen activity.

8. Alumina inclusions tended to be transformed to calcium-rich aluminates by increased calcium treatment, decreased acid soluble aluminum content and decreased sulphur content.

9. A reaction model is proposed to explain the present results. The calcium wire creates a cavity at the injection point. Calcium dissolves into the melt at this point, while oxygen and sulphur diffuse to the cavity and create primary CaO and CaS at the interface. Most of the primary CaO and CaS are eliminated from the melt, but some are entrained into the melt. Reactions with aluminum, manganese, sulphur and oxygen continue at the inclusion interfaces.

10. The calcium recovery was found to vary with time and the calcium injection rate. The total calcium recovery is not a good measure of the extent of inclusion modification.

1.0 INTRODUCTION

Despite the fact that calcium treatment of steel is wide-spread in Canada, the results obtained are often erratic. While some of this may be attributable to variations in steelmaking practice, most of the problem is related to the fact that the mechanisms by which calcium dissolves, desulphurizes, deoxidizes and transforms sulphide and oxide inclusions are largely unknown.

There have been a number of studies on the thermodynamics of calcium treatment of steel [1-6], but the inclusions observed in practice often differ from that expected from equilibrium. Therefore there is a need to study the kinetics of treatment to determine the way in which bulk concentrations change in the steel and the way new inclusion distribution develop.

The facility and procedures which were developed for these kinetic studies are also well-suited to the preparation of small ingots of calcium-treated steel for property evaluation and for the evaluation of new injection reagents. The facility is available to Canadian Industry for future work.

2.0 EXPERIMENTAL

2.1 APPARATUS

2.1.1 Furnace System

A general view of the vacuum induction furnace facility is shown in Figure 1. The vacuum chamber measures 1 m in diameter by 2 m in length. The vacuum system was only used to evacuate the chamber to be back-filled with argon. One of the sight port was replaced with a 0.1 m ball valve for rapid sampling and oxygen probing. When the valve was open, argon was continually flushed in the argon inlet, through the furnace and out the valve to prevent the ingress of air. The alloy addition chamber on top of the furnace was used to add aluminum and synthetic slag before the calcium wire injection.

Magnesia crucibles (0.18 m diameter by 0.33 m high) were used for the exp riments; the 40 kg charge would fill approximately two-thirds of the crucible.

A welding wire feeder was adapted to feed the steel-clad calcium wire at rates between 0.02 and 0.12 m/s. A guide tube inside the furnace was used to ensure that the wire entered the melt without bending.

2.1.2 Oxygen Measurements in the Furnace Atmosphere

The furnace atmosphere was intermittently monitored with a portable oxygen analyzer (Teledyne, Model 320P-4) which uses a pump to aspirate a sample from the furnace. The sample is passed through a fuel cell to provide a direct reading of volume per cent oxygen. Its accuracy is ±5% of reading or ±1% of full-scale.

2.1.3 Oxygen Activity in Molten Steel

Commercial, single use electrochemical oxygen cells (Electro-Nite, Celox2/C11) were used to measure oxygen activity before, during and after injection. The cell consists of a zirconia solid electrolyte, partially stabilized with MgO and several other minor oxides, in contact with a Cr/Cr_2O_3 reference electrode. If the cell operates reversibly, solely by oxygen ionic conduction the oxygen activity is related to the cell potential by:

$$\log a_0 = \frac{-(13580 - 10.08\,E)}{T} + 4.62 \qquad (1)$$

In practice, electronic conductivity cannot be ignored, and is usually accounted for as [7]:

$$E = \frac{RT}{nF} \ln \frac{P_e^{1/4} + \left(P_{O_2}^{II}\right)^{1/4}}{P_e^{1/4} + \left(P_{O_2}^{I}\right)^{1/4}} \qquad (2)$$

where $P_{O_2}{}^{I}$ and $P_{O_2}{}^{II}$ are the oxygen potentials at the cathode and anode, respectively and P_e is the equivalent oxygen pressure due to electronic conduction which must be measured for each cell composition.

Figure 2 shows a comparison between ionic conduction and ionic plus electronic conduction. A calibration developed by CRM and Electro-Nite is also shown. At low oxygen

activity the electronic conductivity dominates. In the present experiments the lowest oxygen activity was 10 ppm, consequently the differences between these relationships are approximately 30%.

2.2 MATERIALS

The steel used for these experiments was AISI 1045, very kindly supplied by Stelco Inc. The nominal composition is 0.45% C, 0.75% Mn, 0.08% P, 0.017% S, 0.25% Si, 0.015% Cu, 0.011% Ni, 0.027% Cr, 0.003% Mo, and 0.027% Acid Soluble Aluminum.

The steel-clad calcium wire (Pfizer Inc.) consisted of pure calcium wrapped with steel. The outer diameter of the wire was 5 mm, and contained 0.0231 kg of calcium per meter.

A 30% lime-70% fluorospar mixture was used as a synthetic slag for some injections, which was donated by Foseco Canada Limited.

2.3 CHEMICAL ANALYSIS

2.3.1 Total Aluminum and Calcium

The total aluminum and total calcium in the steel were analysed with an inductively coupled argon plasma spectrometer equipped for solid sampling (Jarrell-Ash ICAP 7000). Spectroscopic disks are sparked with an arc, but the ablated material is passed through a tube to an RF plasma generator which excites the individual elements in the material. The separation of the sparking and excitation increases the linearity of the calibration compared to the conventional arc-spark mode.

The reliability of the analysis depends on the standards available. In the present study, calcium standards from Brammer Scientific were used for calcium, and National Bureau of Standards reference materials were used for 24 elements including aluminum. Excellent agreement in total calcium content was achieved between this technique and atomic absorption analysis performed by Algoma Steel Corporation.

2.3.2 Acid Soluble Aluminum (ASA)

Acid soluble aluminum is supposed to be a measure of the dissolved aluminum in the steel, however some aluminum compounds such as aluminum nitride are also acid soluble. There are also a variety of techniques employed throughout the industry [8] to determine ASA. Therefore one should carefully interpret ASA analytical results.

The present ASA analyses were kindly performed by Stelco Inc. according to their standard procedure: the steel sample is dissolved in a dilute mixture of hydrochloric and nitric acid which should not dissolve inclusions. After filtering, the solution is aspirated into an inductively coupled plasma spectrometer for aluminum analysis.

2.3.3 Total Sulphur and Oxygen

The total sulphur and total oxygen analyses were performed by combustion analysis on Leco Instruments, 518 and TC-136, respectively.

2.4 INCLUSION ANALYSIS

Quantitative inclusion analysis according to size and composition were performed by Stelco Inc. Their system consists of a scanning electron microscope and a LINK System (860 Series 2) Analyser equipped with both DIGIMAP and DIGISCAN hardware.

Inclusion size and chemical classification are obtained from the DIGISCAN/FDC program. A back-scattered electron image is obtained from the area of interest. The inclusions are identified by setting upper and lower thresholds for the image. Based on the selected thresholds, the inclusions are set white and the matrix black. The LINK digital beam control system moves the beam to the inclusions only. As the beam scans, the size and chemical information for each inclusion are obtained. The area fraction occupied by each chemical class of inclusion and each size range can then be calculated. The chemical classes of inclusions are determined by the user.

2.5 EXPERIMENTAL DESIGN

The most important independent variables were considered to be the sulphur content, the acid soluble aluminum and the calcium feed rate. Table I shows the aim values for these variables, along with the value actually obtained. There were two levels of sulphur: 0.017 and 0.005% S, three levels of acid soluble aluminum: 0.01, 0.05 and 0.10% ASA, and three wire feeding rates: 0.02, 0.06 and 0.10 m/s. Generally 10 m, (0.231 kg Ca), was fed, so that the injection time varied inversely with the feed rate.

TABLE I

EXPERIMENTAL DESIGN OF CALCIUM WIRE INJECTION

Ca Feed Rate (m/s)	0.02	0.06	0.10
ASA (%)	0.01	0.05	0.10
S (%)	0.005	0.017	

2.6 PROCEDURE

Bar stock was charged to the crucible for melting. As the steel was heated, the air was pumped out of the furnace. Close to the melting point of the steel, the chamber was back-filled with argon. Argon was continually flushed through the furnace when the sampling port was open. After melt-down, the power was adjusted to maintain 1600°C. Additions (aluminum and slag) were made through the alloy addition chamber. An initial oxygen probe measurement, chamber oxygen reading and an ingot dip sample were taken.

For the wire feeding, one person controls the wire feeder and takes records on a tape recorder, another takes samples every 30 seconds and makes at least two oxygen probe readings, while the third person assists with sampling. The wire feeding time varies between 1.2 and 7 minutes depending on the feed rate, but samples were also taken for 30 minutes after the injection.

The temperature readings from the oxygen probes were double-checked by single-use thermocouples. Oxygen measurements in the furnace atmosphere were taken frequently throughout the experiment.

A second injection usually followed the first one, in which case the starting sulphur content would be significantly lower. For the second injection, the melt would be deoxidized with aluminum. After the injections were finished, the ingot would be solidified in the crucible. A new crucible was used for each melt because the splash around the perimeter of the crucible was hard to separate.

3.0 RESULTS

A summary of the initial experimental conditions for the injections is shown in Table II for the 12 successful ones. The results for the bulk chemical analyses will first be presented, followed by the micro-analysis of the inclusions.

3.1 BULK CHEMICAL RESULTS

Typical results obtained for injections without any synthetic slag are shown in Figure 3. The total calcium content increase to approximately 70 ppm, and remains constant. The oxygen activity decreases slightly to approximately 10 ppm, while the total oxygen content increases from 20 to 35 ppm. There is a considerable amount of desulphurization in his heat starting with 0.025% S. The ASA declines indicating that soluble aluminum is consumed, however the total aluminum is constant. This is reasonable since there was no synthetic slag to absorb the inclusions produced during injection.

Figure 4 shows typical results for injections with a synthetic slag cover at similar feed rate as in Figure 3. The trends are similar except for the decrease in total aluminum which could be attributed to the absorption of inclusions in the slag.

After wire feeding the calcium content decreases very rapidly, while the oxygen activity increases. In general at the end of injection, most the slag has been ejected from the melt surface, except around the perimeter of the crucible. Consequently, reoxidation from the atmosphere and calcium evaporation can occur. The rapid decrease of both total and acid soluble aluminum can be attributed to reoxidation as well.

3.2 INCLUSION DISTRIBUTION AND CHEMICAL ANALYSIS

In the inclusions, the only elements detected in concentrations greater than 5% were Fe, Ca, Al, Mn and S. (There were trace amounts of Si, Ti, Mg and so on). The inclusions were divided into classes according to Table III. The 5% threshold was chosen as the lower limit for classification of the major components. The right-hand column of Table III identifies the stoichiometric compounds which fall into each classification. CaS and MnS form a range of solutions depending on temperature as shown in the binary phase diagram, Figure 5. There are also a number of calcium aluminates, as illustrated in the $CaO\text{-}Al_2O_3$ phase diagram, Figure 6.

All of the inclusions found in this study were spherical and less than 20 μm in diameter. Typically the inclusions were composed of more than one phase, so that the designations in Table III apply to the average inclusion composition. Typical optical micrographs of inclusions appear in Figure 7A and 7B. The size distribution of the inclusions is shown in Figure 8.

3.2.1 Area Fractions of Inclusions

The area fraction of the classes of the inclusions are shown in Figure 9 during one injection as the calcium content increases. The CaS and CaO contents increase rapidly, while the $CaS\text{-}CA_x$ increases less rapidly. The amount of MnS and Ca(Mn)S decrease as the calcium content increases. (As will be shown later the calcium content of the Ca(Mn)S also increases).

For a constant calcium content of 0.01% Ca, the inclusion distribution is shown in Figure 10. This data is from one injection in which the sulphur content decreased with time. The sulphur containing phases decreased with sulphur content. The lime area fraction first decreases, and then increases.

TABLE II

SUMMARY OF EXPERIMENTAL CONDITIONS

Heat & Run (No.)	Weight of Melt (kg)	Ca Feed Rate (kg/T min)	Injection Time (Min)	Ca FED (g)	Initial Conditions							
					Total Al (%)	ASA (%)	Oxygen Activity (ppm)	Total Oxygen (%)	Chamber Oxygen (%)	Sulphur Content	Foseco Slag (g)	Initial Temp (°C)
H3R1	36.86	0. 795	6.35	176.00	0.1339	0.127	2.47	0.0025	1.50	0.028	0	1582
H4R1	37.20	0.842	4.75	144.78	0.0403	0.046	4.20	0.0025	0.08	0.014	250	1600
H5R1	32.00	4.851	1.16	180.07	0.0278	0.031	8.38	0.0044	0.22	0.008	675	1598
H6R1	40.00	0.906	6.00	217.60	0.0137	0.010	18.60	0.0028	0.07	0.018	250	1585
H6R2	35.00	2.289	2.70	216.44	0.0844	0.078	*	0.0022	0.20	0.003	250	1644
H7R1	41.00	2.299	2.93	277.20	/	/	185.09	0.0095	0.06	0.0189	250	1640
H7R2	38.00	1.036	4.18	164.80	0.0767	0.073	4.88	0.0040	0.30	0.0106	250	1635
H8R1	41.00	2.11	1.90	164.70	/	0.002	35.78	0.0047	0.05	0.012	250	1612
H8R2	38.00	2.25	2.13	182.87	/	0.002	11.62	0.0036	0.70	0.0089	250	1626
H9R1	41.00	3.48	1.83	261.25	0.0028	0.004	61.58	0.0032	0.08	0.0154	250	1642
H9R2	38.00	0.835	4.75	150.76	0.0084	0.01	26.40	0.0049	3.00	0.0013	250	1601
H9R3	33.00	0.832	5.95	163.28	0.1220	0.125	1.47	0.0029	2.40	0.0004	250	1605

Notes: / Not measured
* Below level of detection

TABLE III

DESIGNATIONS OF INCLUSION CLASSIFICATIONS

Element / Designation	Ca	Al	Mn	S	Stoichiometric Compounds
	%				
MnS	0-5	0-5	5-100	5-100	MnS
Al_2O_3	0-5	5-100	0-5	0-5	Al_2O_3
CaS	5-100	0-5	0-5	5-100	CaS
CaO	5-100	0-5	0-5	0-5	CaO
Ca (Mn) S	5-100	0-5	5-100	5-100	CaS + MnS*
CAx	5-100	5-100	0-5	0-5	CA_6, CA_2, CA $C_{12}A_7$ & C_3A†
CaS · CAx	5-100	5-100	0-5	5-100	CaS + CA_x
CaMnS · CAx	5-100	5-100	5-100	5-100	Ca (Mn) S + CA_x

* See CaS-MnS Phase Diagram, Figure 5
† See CaO-Al_2O_3 Phase Diagram, Figure 6

For three different injections with similar sulphur and calcium contents, the effect of acid soluble aluminum is seen in Figure 11. Increased acid soluble aluminum increases both aluminum activity and decreases oxygen activity. This favours the formation of aluminates and sulphides.

The inclusion area fractions for one injection are shown in Figure 12. The most dominant feature of this diagram is the rapid increase and then decrease of the pure Ca0 and CaS inclusions. The calcium aluminate inclusions also shows this trend, while the manganese containing inclusions are in continuous decline. The total area of inclusions also demonstrates a rapid increase and then decrease as shown in Figure 13. As will be discussed later, this phenomenon is probably due to formation of CaO and CaS at the point of injection which are then entrained into the melt.

3.2.2 Chemical Analysis of Inclusions

The calcium content of the Ca(Mn)S inclusions increased with the calcium content during injection (Figure 14). With reference to the CaS-MnS phase diagram, Figure 5, one sees that sulphides with greater than 60 at% CaS are completely solid at 1600°C. For the conditions in Figure 14 this would occur for calcium contents greater than 60 ppm Ca.

The effect of the acid soluble aluminum content on the calcium content of the the Ca(Mn)S containing inclusions at points with the same bulk calcium and sulphur contents in Figure 15. The reduced oxygen activity associated with higher aluminum levels favours CaS over MnS formation.

The calcium content of the CA_x inclusions during the course of injection and the subsequent holding period is shown in Figure 16. The bulk calcium content of the steel is also superimposed. It is clear from this diagram that for even one injection condition that there is no unique relation between total calcium in steel and the extent of transformation of alumina inclusions. For example, 20 ppm Ca early in the injection corresponds to an average inclusion composition near CA_2, while in the holding period 20 ppm calcium corresponds to C_3A. Therefore the kinetics or the history is an important factor in inclusion transformation.

In Figure 17 the calcium content of the CA_x inclusions is plotted against the bulk total calcium content. The present results show that it is possible to "over-treat" heats with calcium and produce calcium aluminate inclusions which are solid because they are too rich in calcium. The phase diagram for the aluminates, Figure 6, shows that inclusions richer than C_3A will contain solid lime at 1600°C. Hilty and Farrell [9] calcium-treated 100 kg air melts of steel; their data is also shown in Figure 17. Given the differences in treatment method, steel chemistry, atmospheric control and inclusion analysis techniques the agreement between the data is reasonable.

For different injections with similar bulk calcium and sulphur contents the effect of the acid soluble aluminum content on the calcium content of the calcium aluminates is shown in Figure 18. The increased aluminum activity at higher ASA increases the aluminum content of the calcium aluminates. While aluminum (or some other deoxidant) must be added to steel, too much aluminum can prevent the formation of liquid calcium aluminates as this diagram shows for these particular conditions.

The effect of sulphur content on the transformation of CA_x inclusions is shown in Figure 19. This behaviour is a result of the relationship between sulphur content and oxygen activity in the present system which is shown in Figure 20. Therefore as the sulphur content is decreased there is less sulphur available to form CaS, and the oxygen activity drops. This latter factor encourages the formation of lime-rich aluminates.

3.2.3 Comparison between Bulk Chemical and Inclusion Analysis

In principal it is possible to calculate the content of each element contained as inclusions from the number, size and composition of the inclusions. The contents of each element in inclusions can be subtracted from the total bulk analysis to obtain the content of the element dissolved in the steel. There are a number of difficulties in actually performing this calculation. First of all, there are uncertainties in the number, size and composition of the inclusions because it is only practical to analyse a small fraction of the sample. (In the present study, 20 fields each measuring 94 μm by 94 μm were taken from one polished sample). Another problem is that there is a distribution of particle sizes which are randomly sliced by the metallographic section. Some particles may be sliced through their largest cross-section, but it is more likely that a smaller cross-section is cut. Therefore a statistical correction procedure is required to adjust the observed particle distribution. In the present case, Underwood's procedure is used [10].

The results of this calculation are summarized in Table IV. The calcium content in inclusions is generally greater than the total calcium content measured by bulk chemical analysis. Obviously this cannot be the case, and it is probably due to the above-mentioned uncertainties. However one can say that most of the calcium in the steel is tied up as inclusions. A similar problem exists with this calculation for oxygen, again an indication that most of the oxygen is in inclusions. It is only for the sulphur analysis that there is a large enough difference between the total sulphur and the sulphur in inclusions, to say that there is some dissolved sulphur.

TABLE IV

COMPARISON BETWEEN CHEMICAL AND INCLUSION ANALYSIS

Element†	H6R1 #8	H6R1 #11	H6R1 #13	H6R1 #16	H6R1 #18	H6R1 #19	H9R1 #4	H7R1 #7
Ca_{tot}†	0.0042	0.0071	0.010	0.010	0.010	0.0013	0.0071	0.0071
Ca_{inc}	0.0069	0.0081	0.0133	0.0083	0.0091	0.0038	0.0044	0.0093
Ca_{dis}	–	–	–	0.0017	0.0009	–	0.0027	–
$O_{tot} - a_o$	0.0018	0.0020	0.0026	0.0027	0.0013	0.0016	0.0011	0.0020
O_{inc}	0.0010	0.0009	0.0023	0.0012	0.0054	0.0005	0.0012	0.0053
S_{tot}	0.0100	0.0100	0.0090	0.0060	0.0040	0.0020	0.0110	0.0085
S_{inc}	0.0040	0.0053	0.0058	0.0040	0.0017	0.0018	0.0020	0.0043
S_{dis}	0.0060	0.0047	0.0032	0.0020	0.0023	0.0002	0.0090	0.0042

†: tot: total amount of element analyzed by chemical method
inc: amount of element combined in the inclusions analyzed by inclusion counting and calculation
dis: amount of dissolved element or the difference between above two quantities
$O_{tot} - a_o$: total oxygen minus the oxygen activity.

3.3 CALCIUM PICK-UP RATES

Typically the total calcium content increased rapidly at the beginning of injection, and reached a steady-state value as shown in Figure 21. One sees that both the pick-up rate and steady-state value increase with calcium feed rate. This suggests that the rate of pick-up is controlled by the rate of calcium dissolution. As noted in the previous section, most the total calcium content was calcium combined as inclusions. This means that the calcium that dissolves is quickly converted to inclusions in the melt. For a dissolution process, the rate of dissolved calcium increase can be expressed as:

$$\frac{d\%Ca}{dt} = K_{DIS}(\%Ca^{SAT} - \%Ca) - K_{EVP}(\%Ca) \qquad (3)$$

where K_{DIS} and K_{EVP} are the rate constants for pick-up and calcium fading, respectively.

By fitting the calcium pick-up curves to this function, apparent values of these parameter were obtained, Figure 22. This diagram shows that the pick-up rate increases rapidly with feed rate, while the fading rate is independent of feed rate.

3.4 CALCIUM FADING RATES

During the holding period after injection, the calcium content decreases rapidly with time. If all the calcium were dissolved calcium, one could write the following expression for the rate of evaporation:

$$\frac{d\%Ca}{dt} = -K_{EVP}\%Ca \qquad (4)$$

According to this relation, if one plots the logarithm of the calcium content against time, a straight line with the slope, K_{EVP} will be obtained. This is done for the <u>total</u> calcium content, which is mainly calcium as inclusions, in Figure 23. The average slope of these lines yields an apparent, first-order rate constant of 5 ± 2.5 X10-4 m/s. This value is two orders of magnitude greater than can be explained by molecular diffusion according to Machlin's Model [11] for evaporation from inductively stirred melts. This means that the elimination rate of calcium containing inclusions from the melt under the present conditions apparently follows first-order kinetics. This will be further discussed with regard to the mechanism in the Discussion.

3.5 DESULPHURIZATION AND DEOXIDATION RATES

The rate of desulphurization and deoxidation both increase with the calcium feed rate as shown in Figure 24. Desulphurization also proceeds to lower levels as the acid soluble aluminum content increases as indicated in Figure 25. The rate of desulphurization was fitted to the following rate expression:

$$\frac{d\%S}{dt} = -K_S\%S \qquad (5)$$

where K_S is the rate constant for desulphurization. This rate constant increases rapidly with calcium feed rate as shown in Figure 26, and furthermore is very similar for the observed K_{DIS} values. The significance of this will be discussed with the mechanism.

4.0 DISCUSSION

4.1 CALCIUM RECOVERY

Calcium recoveries are often quoted for industrial processes as the calcium retained in the melt compared to the calcium injected into the steel:

$$\text{CALCIUM RECOVERY} = \frac{\%\,Ca - \%\,Ca_{INITIAL}}{\%\,Ca_{ADDED}} \qquad (6)$$

In industrial processes this can only be done by comparing calcium before and after injection. In the present experiments the calcium recovery was calculated at each sampling time based on the total calcium content. The results for three different injection rates are shown in Figure 27. The peak is due to the fact that the calcium content increases rapidly at the beginning, but levels off (Figure 21) even though calcium is still being fed. The peak is higher and occurs at shorter times for increased feed rate because K_{Ca} increases with feed rate (Figure 22). Therefore both the feed rate and the sampling time influence the observed values for calcium recovery. Furthermore, the extent of inclusion modification cannot be deduced from calcium recoveries based on total calcium content as Figure 17 demonstrates. In summary, calcium recoveries must be carefully interpreted, and comparisons between widely different practices may not yield a useful measure of the effectiveness of inclusion modification by the different techniques.

4.2 REACTION MECHANISM

In such a complicated system it is difficult to obtain good data, particularly with regard to the inclusion size and composition analysis. Consequently, it is also difficult to develop a comprehensive reaction model. However it is possible to propose a tentative reaction mechanism for the present experimental conditions. Possible implications for full-scale injections are discussed in the next section.

A schematic reaction mechanism diagram is presented as Figure 28. The steel-clad calcium wire is fed into the bath. Based on the work on aluminum wire feeding by Mucciardi [12], it is expected that the penetration depth will be of the order of 0.02 m at a feed rate of 0.01 m/s and will increase with injection rate. The calcium vaporizes at the bottom of the wire, and comes in contact with the steel in the cavity produced by the wire. Because the penetration is so shallow, it is not expected that calcium bubbles would form in contrast to deep, full-scale injection. Consequently, most of the calcium will escape into the freeboard region accounting for the low calcium recoveries (compared to industrial practice).

Some calcium will dissolve through the cavity interface into the steel. At the interface, the equilibrium solubility of calcium in contact with pure calcium vapour is estimated to be 0.024% Ca [5]. The calcium which diffuses into the steel is quickly consumed by reactions with inclusions which accounts for the fact that the total calcium content was almost entirely calcium in inclusions.

While the calcium diffuses into the steel through the cavity wall, sulphur and oxygen can diffuse the cavity and form CaS and CaO at the interface. For convenience, we will refer to these as primary CaS and CaO. Most of the primary CaS and CaO will be carried out of the cavity into the slag or the atmosphere. This is expected to be the dominant mechanism for desulphurization which accounts for the equality of the rate constants for dissolution and desulphurization (Figure 26); both these processes have the cavity interface as the reaction site. Not all the primary CaS and CaO are eliminated from the melt, in fact it is proposed that

this accounts for the large number of CaS and CaO inclusions observed in the melt (Figure 12). The calcium fading will be due to loss of calcium containing inclusions as well as evaporation of dissolved calcium.

Reactions can continue at the inclusions in the melt as sketched in Figure 28. Manganese and sulphur can diffuse to the CaS inclusions to form the Ca(Mn)S inclusions. Aluminum, sulphur and oxygen can diffuse to the CaO inclusions to make the CA_x and $CaS\text{-}CA_x$ inclusions. Inclusions are continually being eliminated from the melt as new one come in from the injection cavity. This accounts for the fact that CaO, CaS and calcium aluminates are found simultaneously which would not be permitted if the melt were at equilibrium. A more quantitative kinetic model is under development.

4.3 COMPARISONS WITH FULL-SCALE PROCESSES

There are several differences between the present experiments and full-scale injection processes. Table V compares the injection rates. While the linear rate of wire feeding is much slower than full-scale, the specific injection rate per tonne is higher. This is due to the small melt volume. Consequently, in the present experiments the amounts of calcium added are greater than full-scale.

TABLE V

	Calcium Feed Rates	
	Linear (m/s)	Specific (kg Ca/tonne/min)
Present work	0.02 – 0.10	0.8 – 4.8
Full-scale	1 – 5	0.02 – 1.0

Again because of the small melt volume the conditions in the present experiments are more characteristic of what would be expected near the injection point in a full-scale process. For example, it is believed that this is the first time that large amounts of primary CaO and CaS have been observed.

5.0 WORKSHOP ON CALCIUM TREATMENT OF STEEL

On February 29, 1988 at McMaster University a Workshop on Calcium Treatment of Steel was held. The results of this project were presented. Dr. D.A.R. Kay of McMaster also made a presentation on his work on machinability. There was also a tour of the facility and a discussion on the problems and future of calcium treatment.

There were approximately 20 industrial representatives from the following companies: Algoma Steel Corporation, Atlas Steel, Dofasco, Inc., Ipsco, Inc., Lasco, Slater Steel Corporation, Stelco, Inc., and Timminco Metals. This final report will be sent to these companies, as well as those interested who could not send a representative to the Workshop.

6.0 REFERENCES

1. D. Sponseller and R.A. Flinn: Trans. AIME, 230, (1964) , pp.876.

2. M. Kohler, H. Engell and D. Janke: Steel Research, (1985), No. 8, pp.413-423.

3. T. Ototani, Y. Katamura and T. Degawa: Trans. ISIJ, (1976), No. 16, pp. 275-282.

4. M. Nadif and C. Gatellier: IRSID Report, June, 1985.

5. D.A.R. Kay and S.V. Subramanian: in Second International Symposium on the Effect and Control of Inclusion and Residuals in Steel, CIM, Toronto, 1986, pp. I25-I43.

6. G.M. Faulring and S. Ramalingam: Metall. Trans. B, (1980), Vol. 11B, pp. 125-132.

7. C. Wagner: in Advances in Electrochemistry and Electrochemical Eng., (1966), Vol. 4, pp.1-46.

8. O.P. Bhargava, G.F. Pitt, J.F. Donovan and W.G. Hines: in Technicon International Congress, Nov. 2-4, 1970, New York.

9. D.C. Hilty and J.W. Farrell: Iron and Steelmaker, (1975), May, pp. 17-20 and June, pp. 20-27.

10. E.E. Underwood: in Quantitative Microscopy, ed. R.T. de Hoft and F.N. Rhines, 1968, McGraw-Hill, New York, p. 149.

11. E.S. Machlin: Trans. AIME, Vol. 218, (1960), pp. 314-26.

12. F. Mucciardi: M.Eng. Thesis, McGill University, 1977.

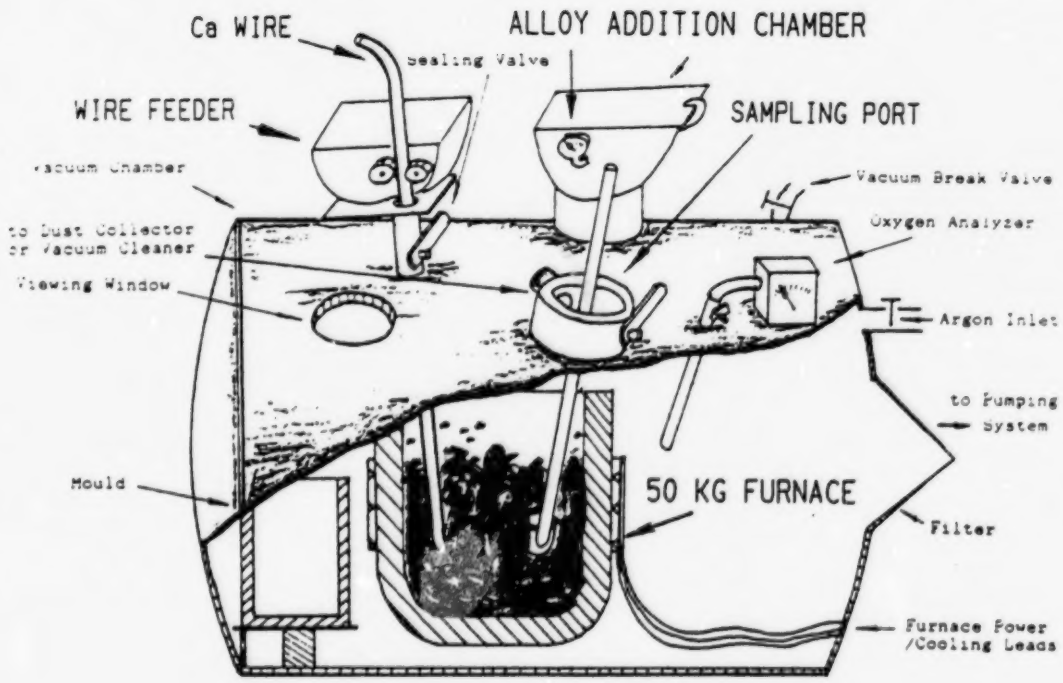

Figure 1: **Schematic view of the vacuum furnace facility showing the injection of wire into the melt.**

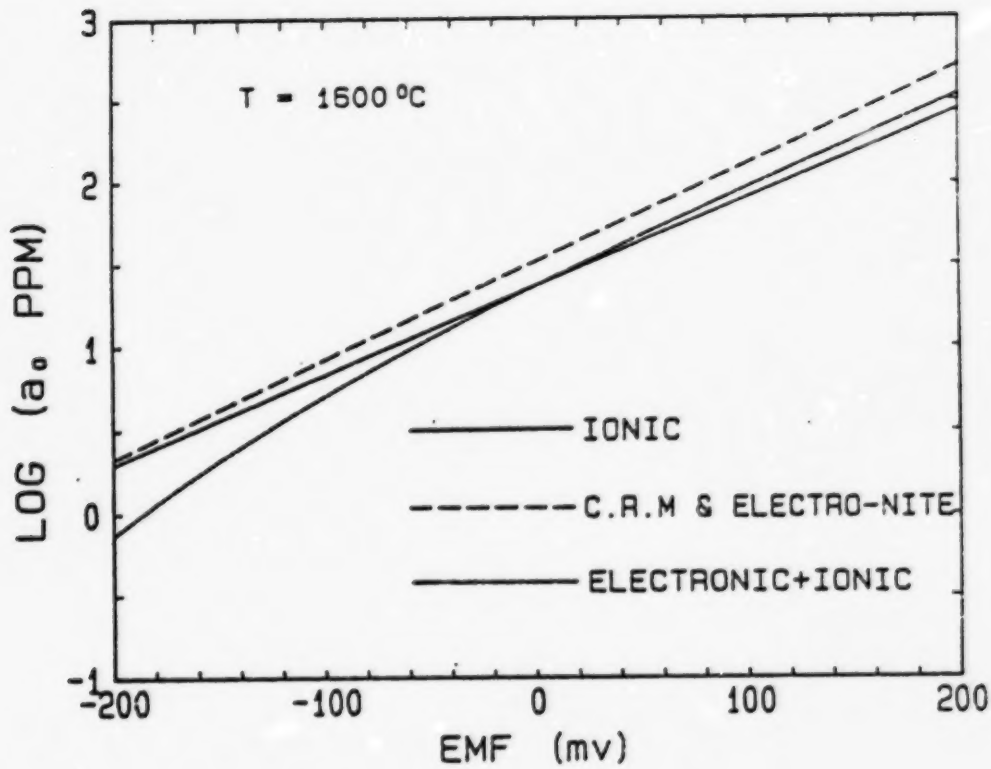

Figure 2: Comparison of oxygen activities calculated from purely ionic conduction, electronic plus ionic conduction and the correlation developed by CRM and Electro-Nite.

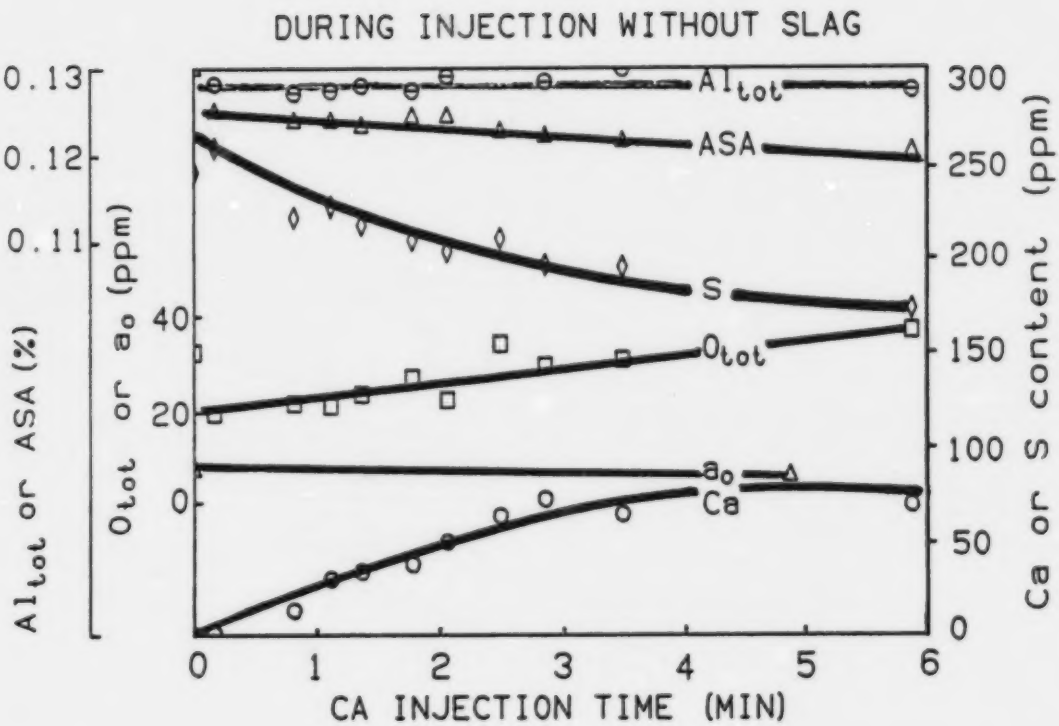

Figure 3: **The changes of total calcium, oxygen activity, a_o, total oxygen, sulphur content, acid soluble aluminum and total aluminum content for an injection without any synthetic slag addition (H3R1).**

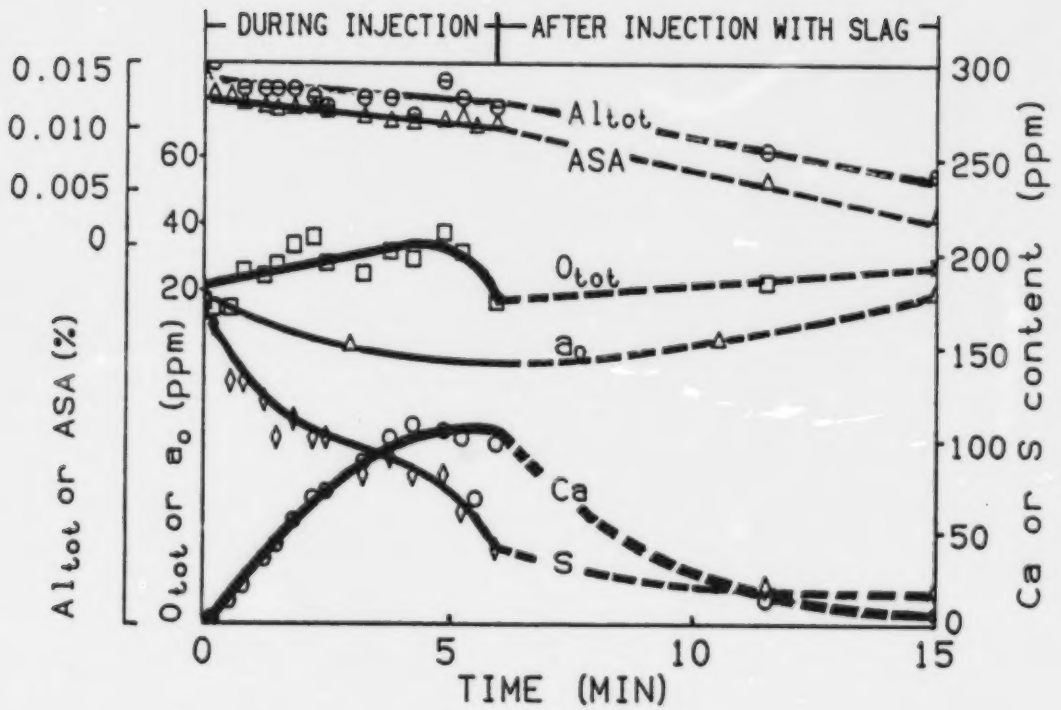

Figure 4: The changes of total calcium, oxygen activity, a_o, total oxygen, sulphur content, acid soluble aluminum and total aluminum content for an injection with a synthetic slag addition (H6R1).

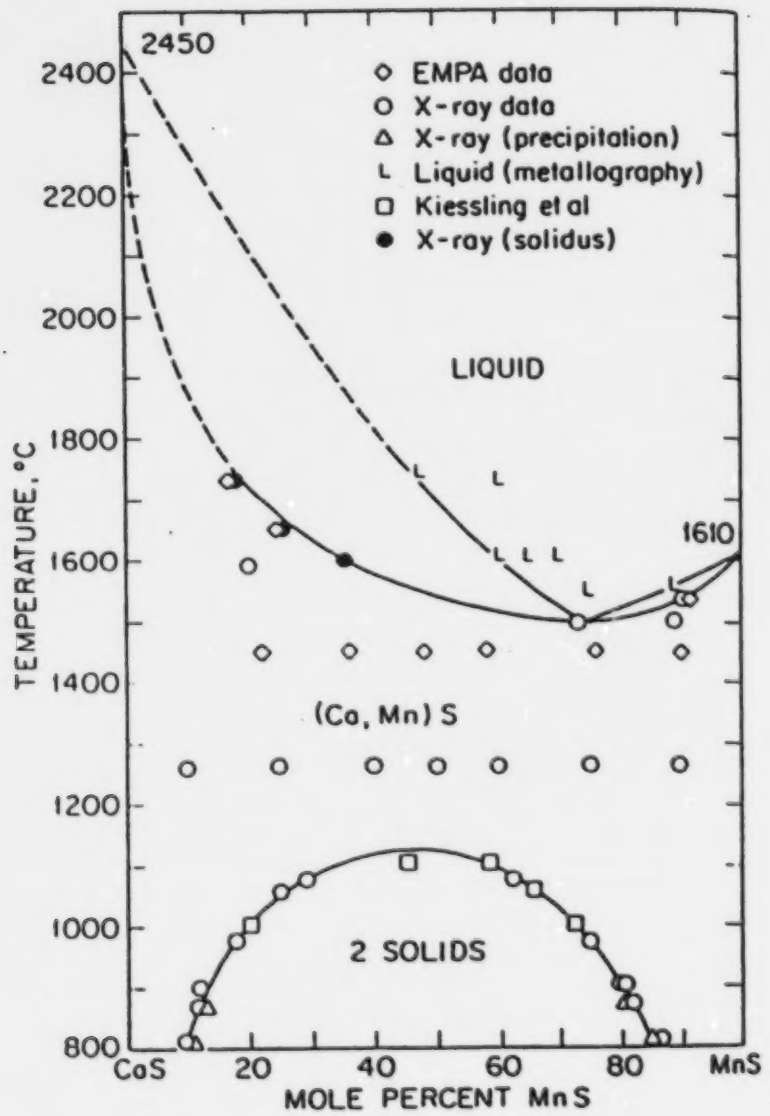

Figure 5: The CaS-MnS phase diagram.

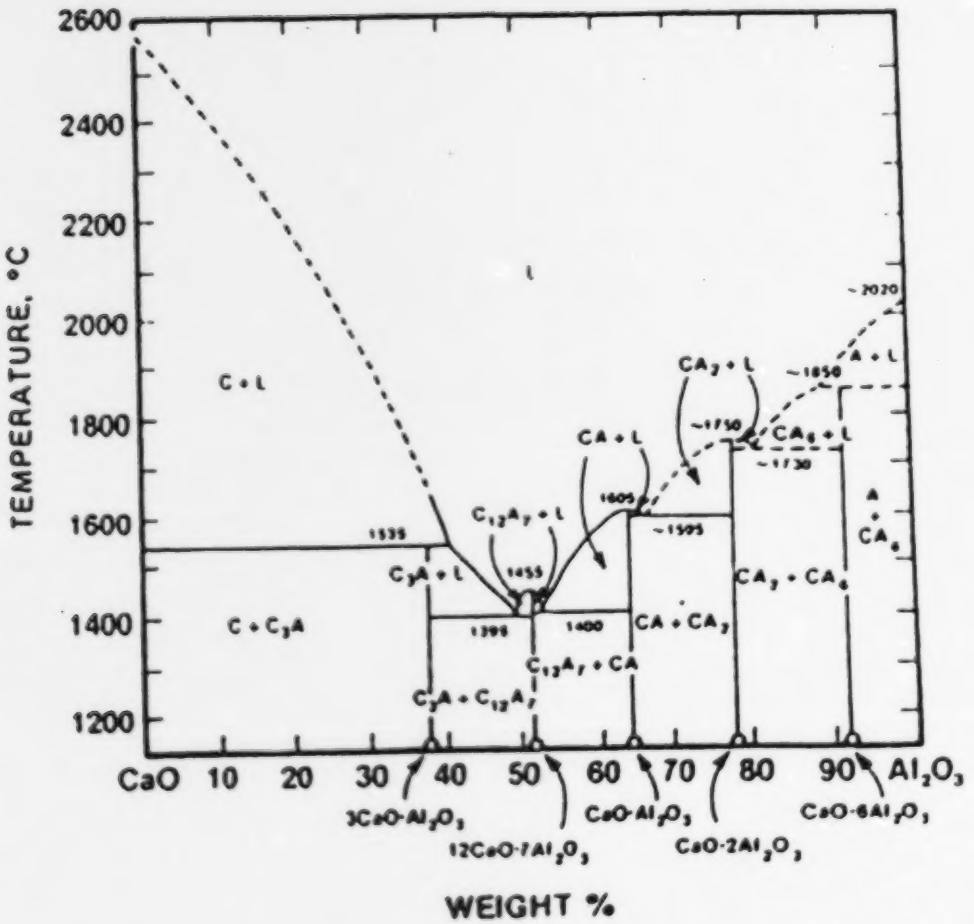

Figure 6: The Al_2O_3-CaO phase diagram.

Figure 7A: SEM micrograph of a sulphide inclusion.

Figure 7B: SEM micrograph of an oxide inclusion.

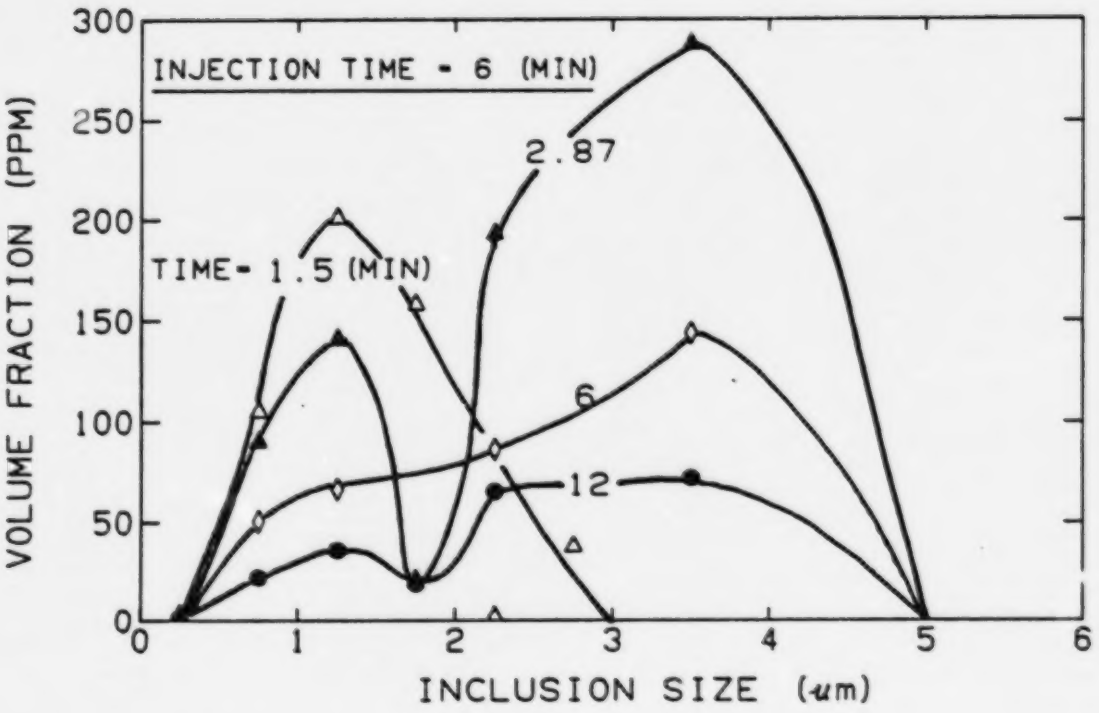

Figure 8: **The size distribution for the inclusions from injection H6R1.**

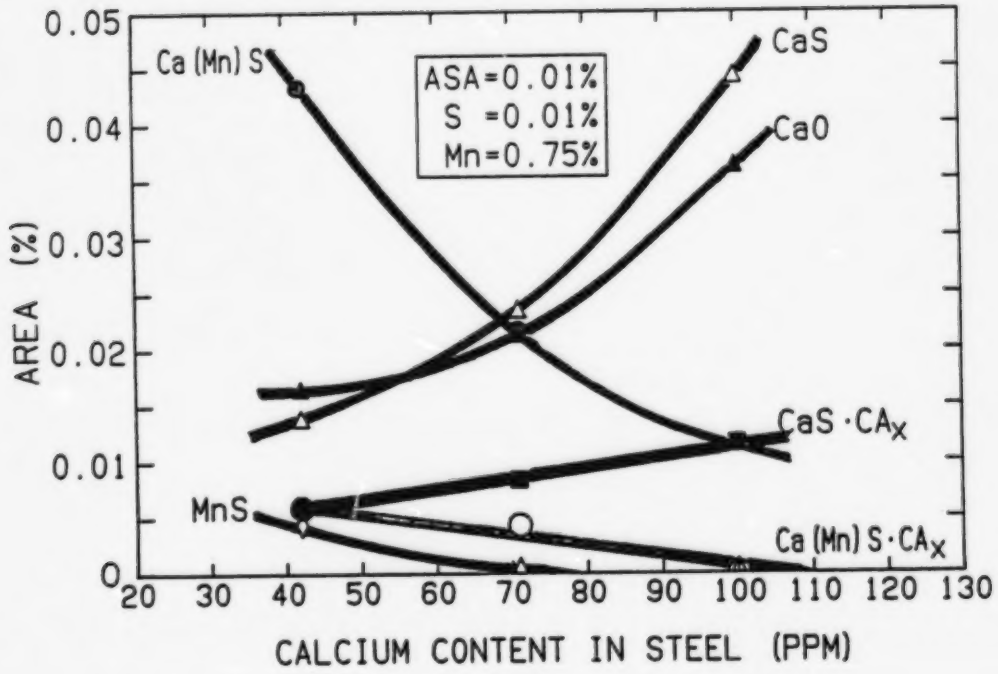

Figure 9: The percentage area (compared to scanned area) of each inclusion type as a function of the total bulk calcium content of the steel for injection H6R1.

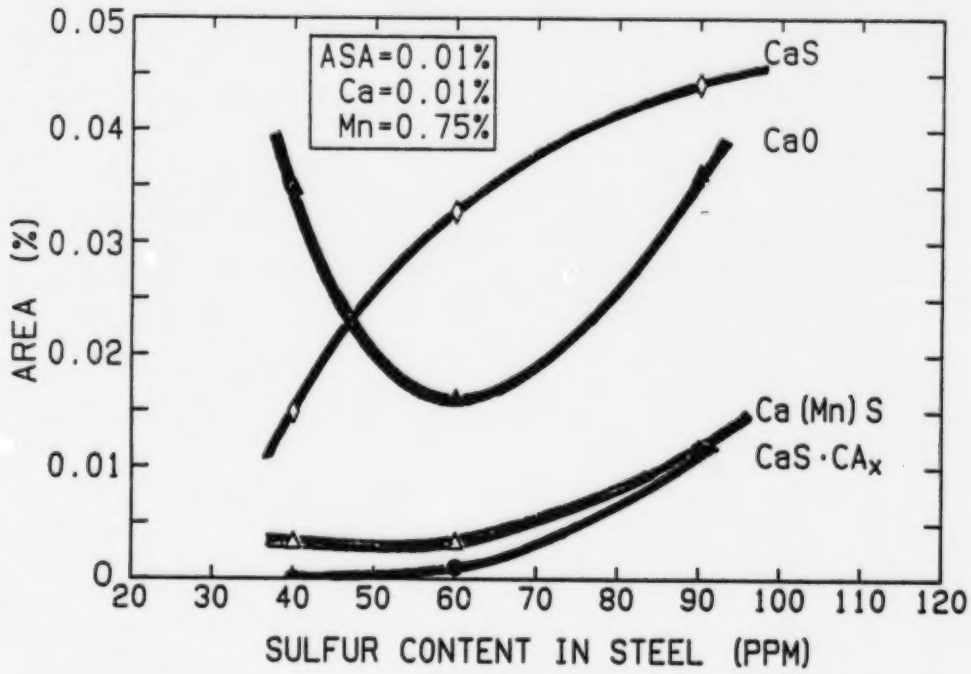

Figure 10: **The effect of sulphur content on the area of the inclusion types during injection H6R1.**

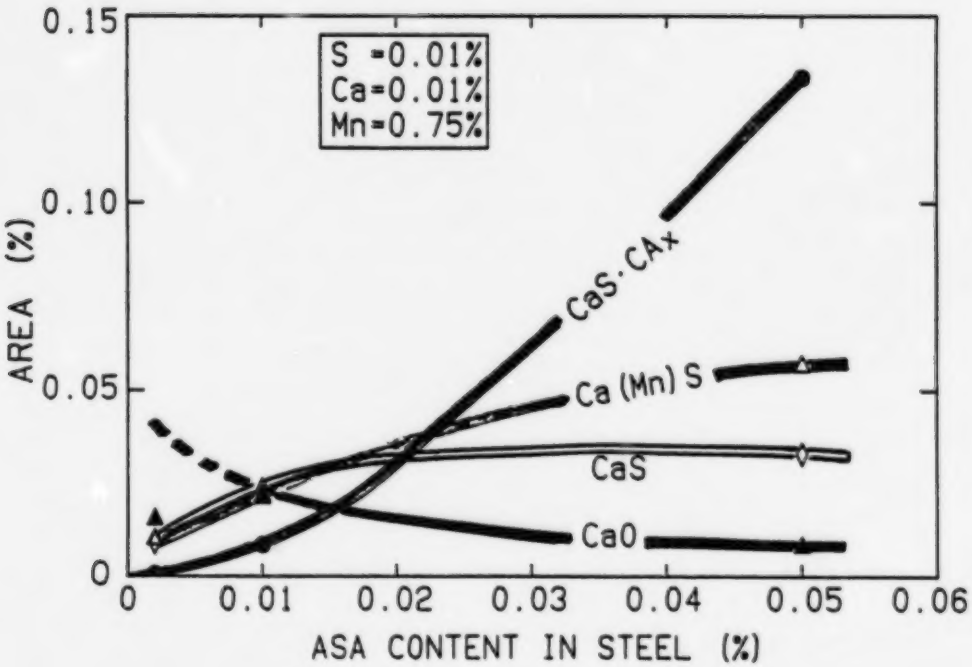

Figure 11: **The effect of the acid soluble aluminum content on the area of each inclusion type.**

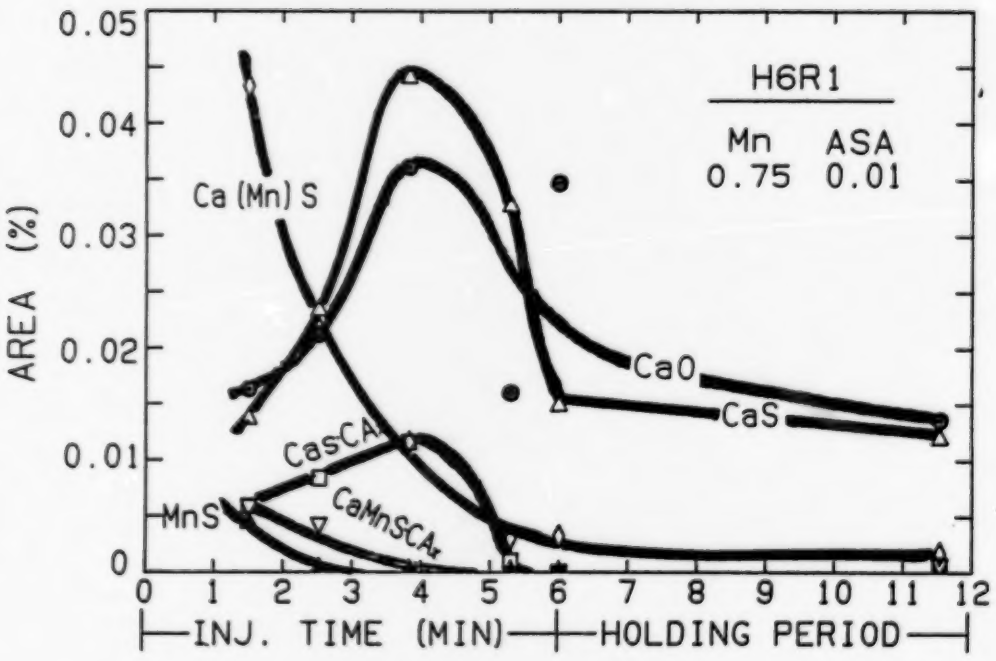

Figure 12: The area of each inclusion type during and after injection H6R1.

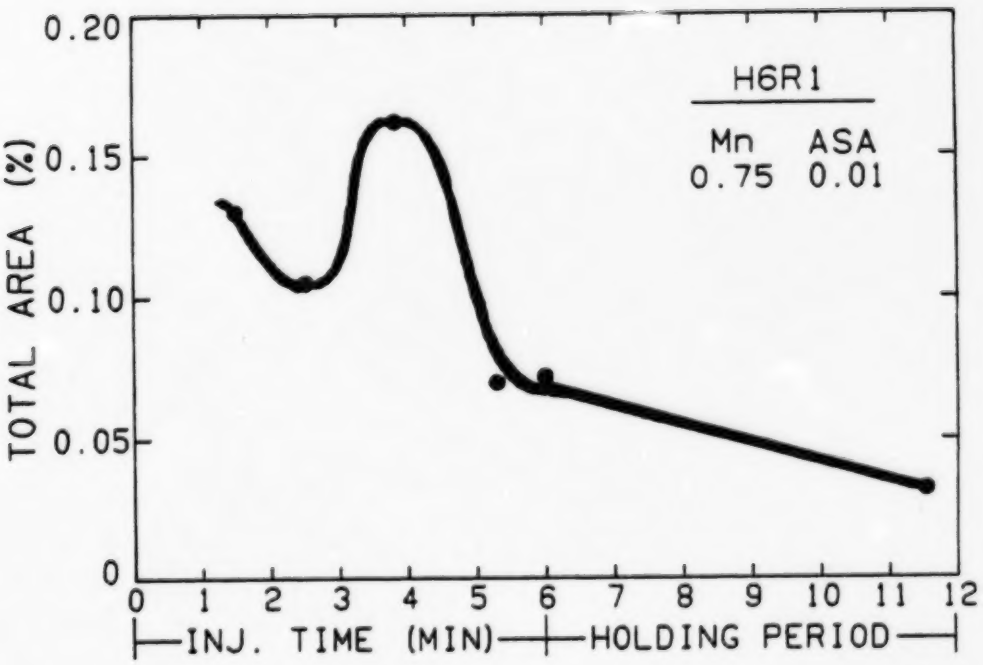

Figure 13: The total area of all inclusions as a percent of the scanned area during injection H6R1.

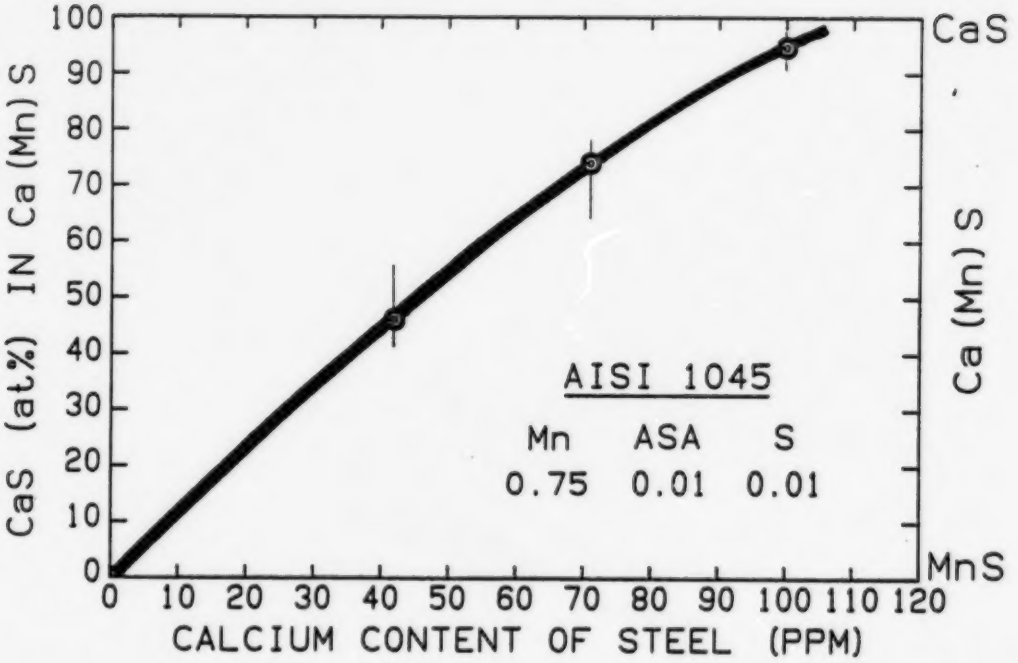

Figure 14: **The calcium content of the Ca(Mn)S inclusions as a function of the total calcium content of the steel during injection H6R1.**

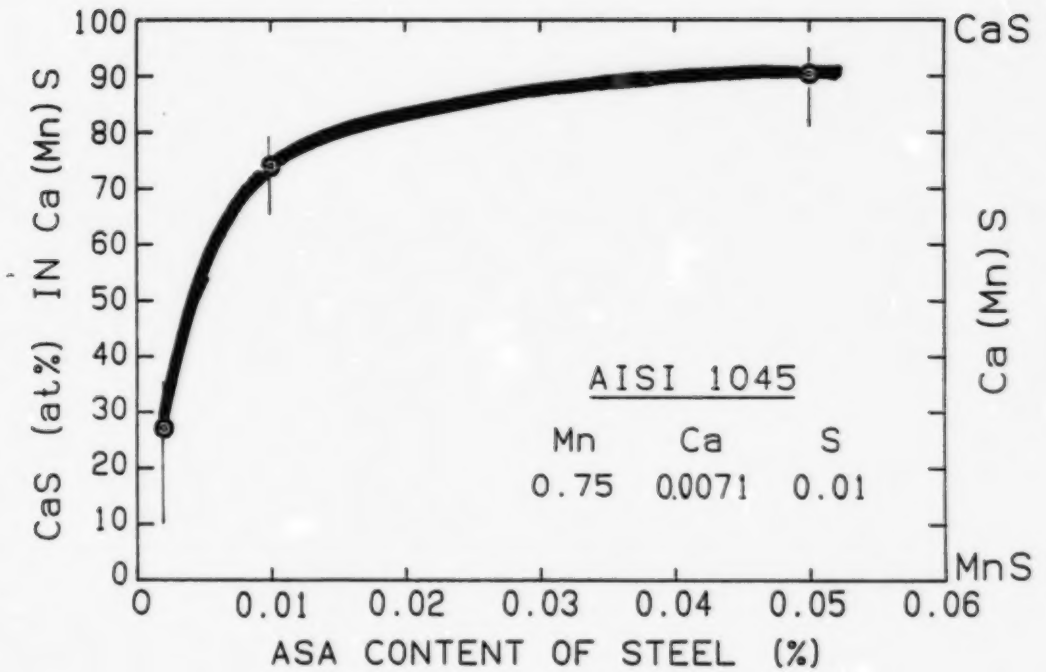

Figure 15: The calcium content of the Ca(Mn)S inclusions as a function of the acid soluble aluminum content of the steel for three different injections.

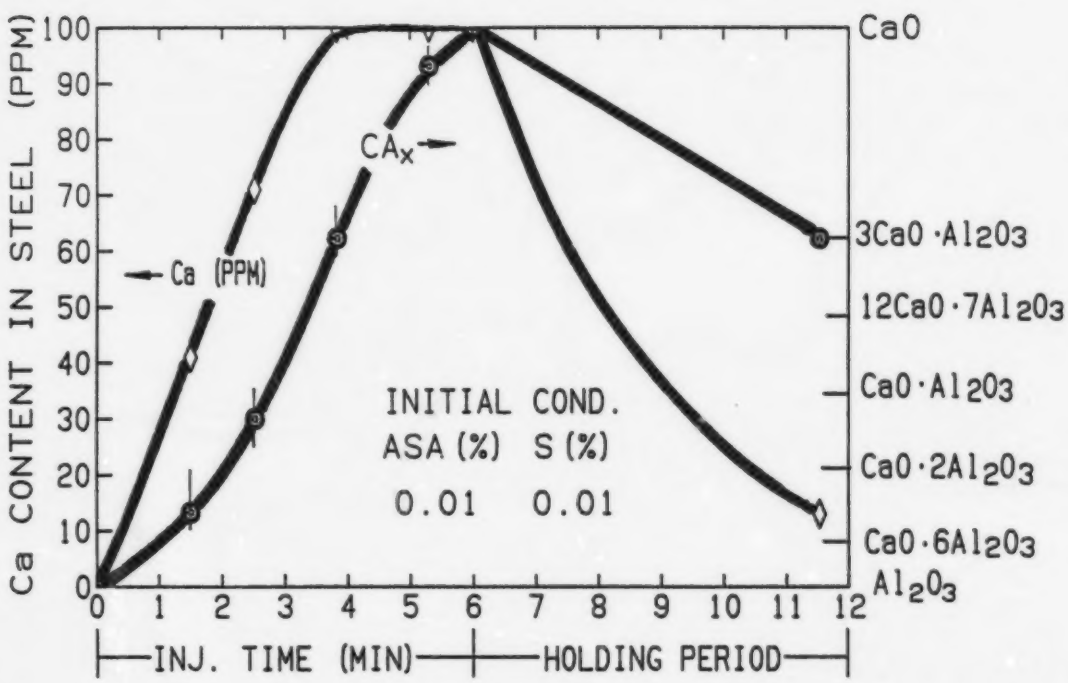

Figure 16: The calcium content of the calcium aluminate inclusions, CA_x, during injection H6R1. The total calcium content of the steel is also shown for the same samples.

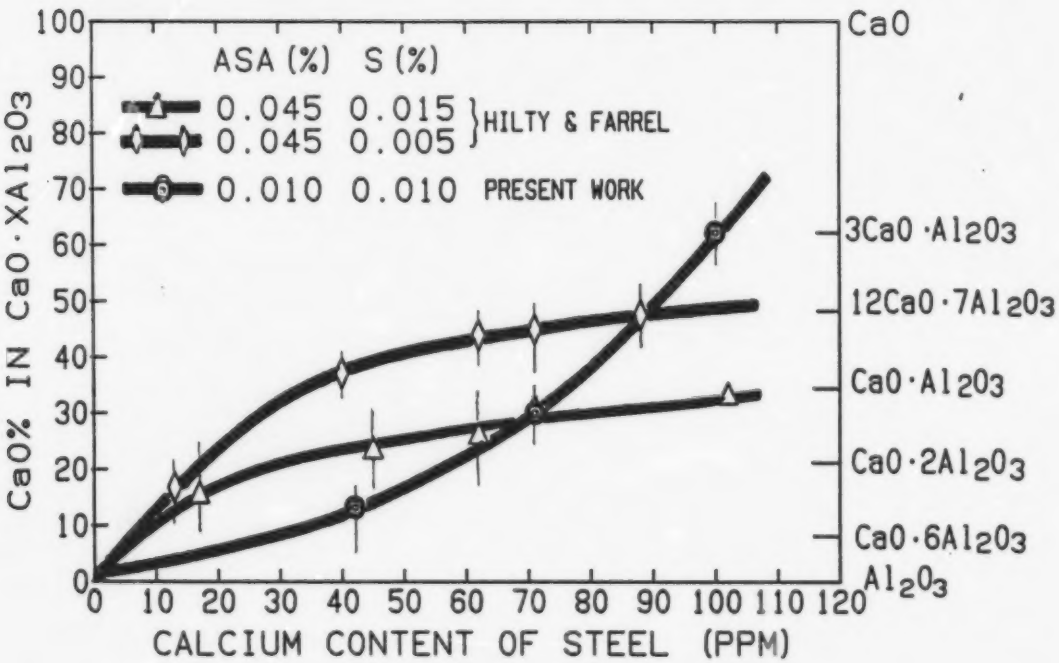

Figure 17: The calcium content of the calcium aluminate inclusions, CA_x, as a function of the calcium content of the steel. The data obtained by Hilty and Farrell [9] are also shown.

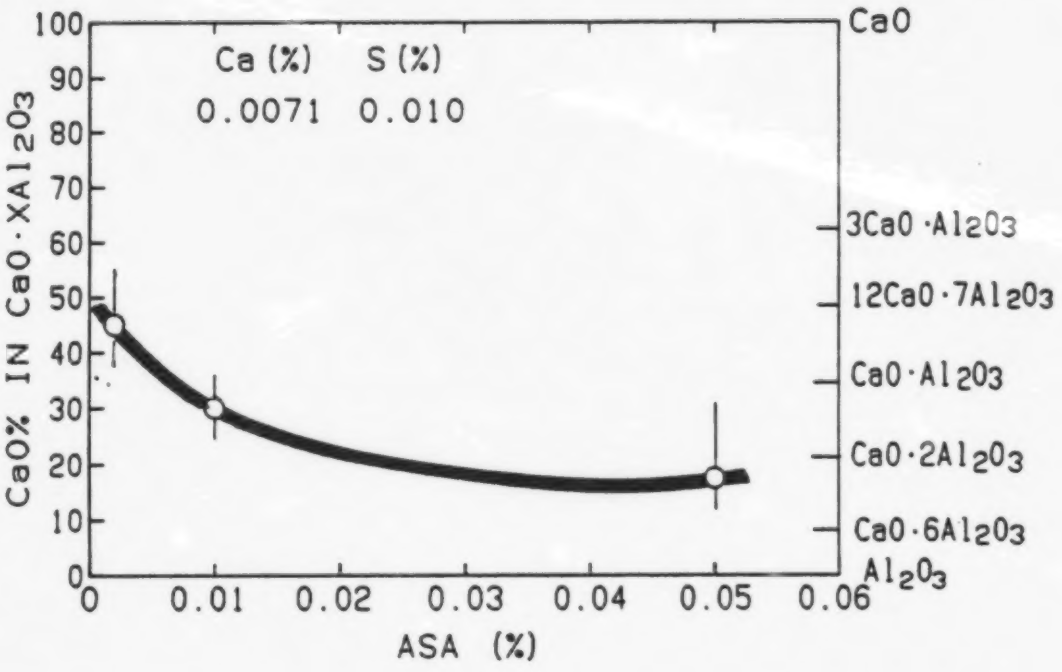

Figure 18: The effect of the acid soluble aluminum content on the calcium content of the calcium aluminate inclusions, CA_x, for three different injections with the same total calcium and sulphur content in the steel.

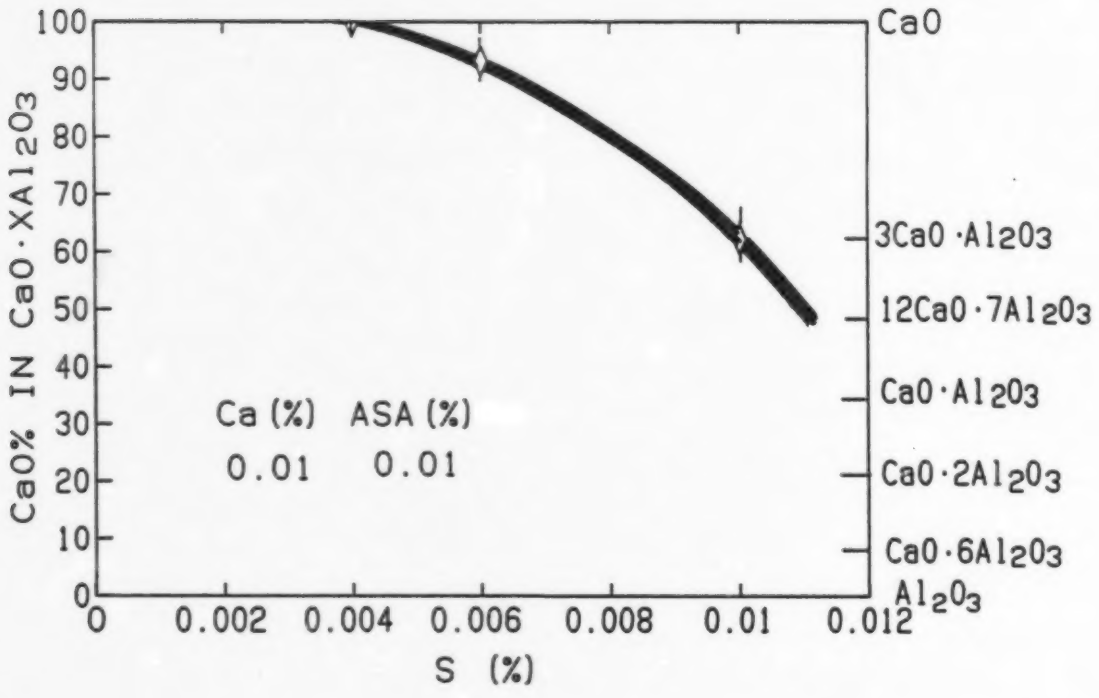

Figure 19: The effect of the sulphur content of the steel on the calcium content of the calcium aluminates, CA_x, for three different injections with the same total calcium and acid soluble aluminum content in the steel.

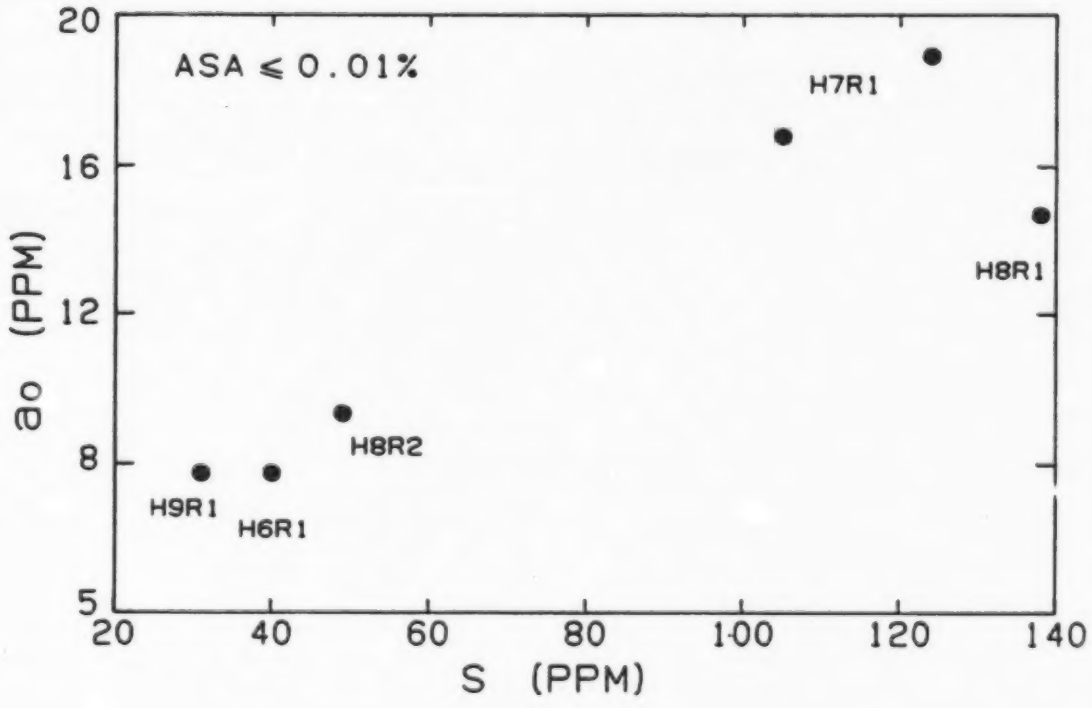

Figure 20: The effect of the oxygen activity measured by the oxygen probe and the sulphur content of the steel.

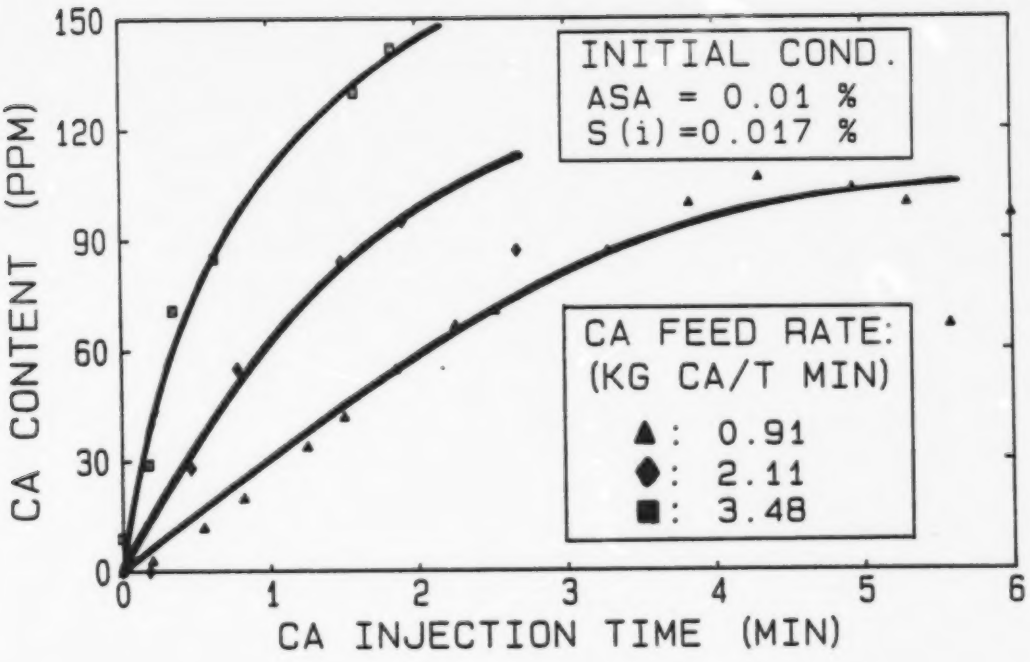

Figure 21: The effect of the calcium wire feeding rate on the rate of total calcium content pick-up in the steel for three different injections with the same initial sulphur content, 0.017 and acid soluble aluminum content, 0.01%.

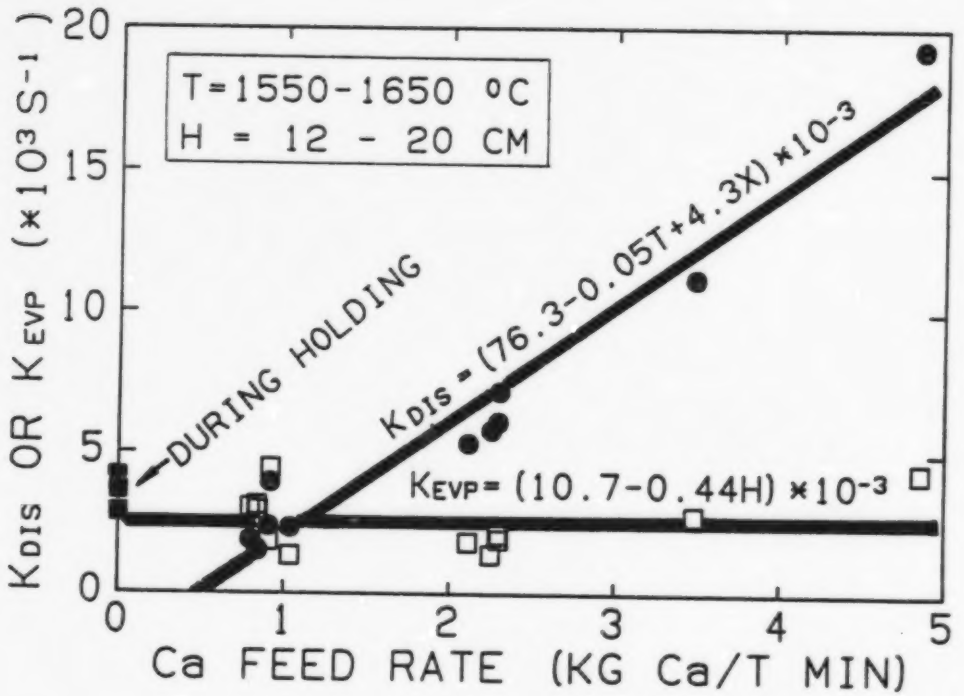

Figure 22: The apparent rate constants for calcium pick-up, K_{DIS}, and calcium fading, K_{EVP}, as a function of the calcium feed rate. The equations represent multiple regressions on the feed rate, melt temperature and melt depth, indicating that the feed rate is the most significant variable.

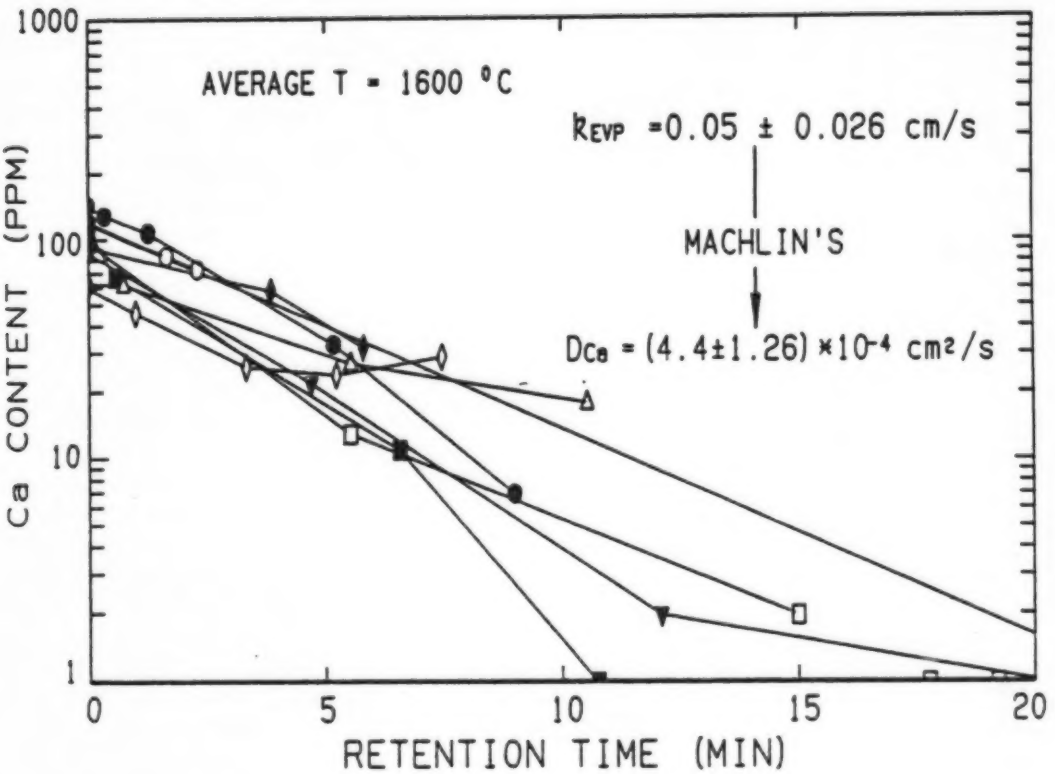

Figure 23: The logarithm of the total calcium content as a function of time after the end of calcium feeding.

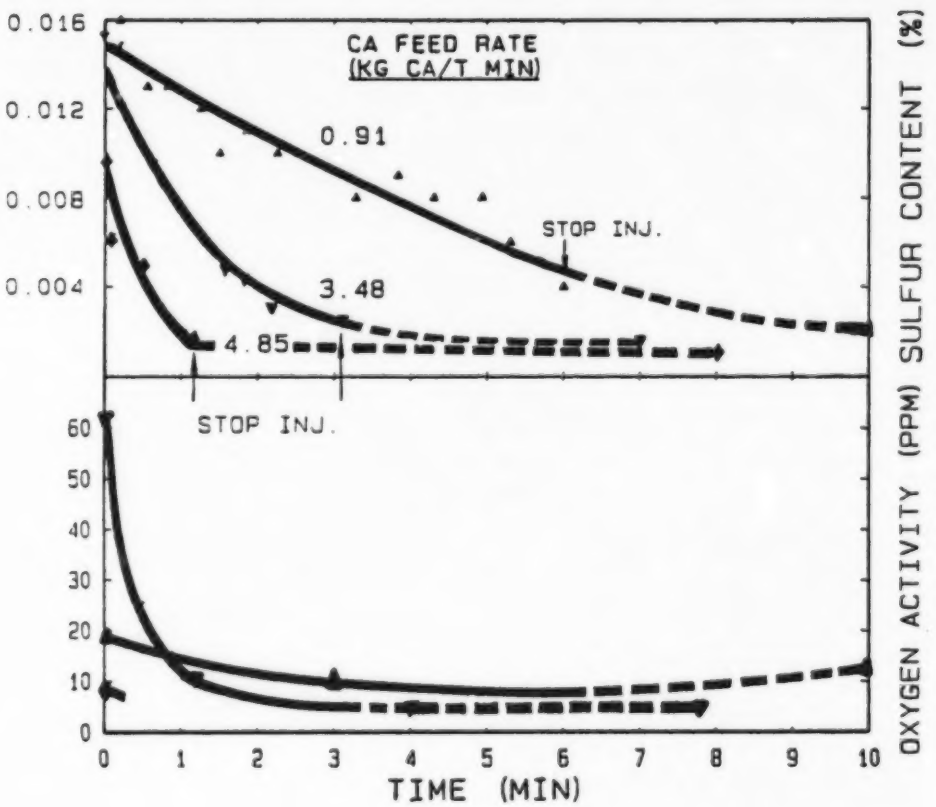

Figure 24: The effect of calcium feed rate on the desulphurization (TOP) and changes in oxygen activity (BOTTOM).

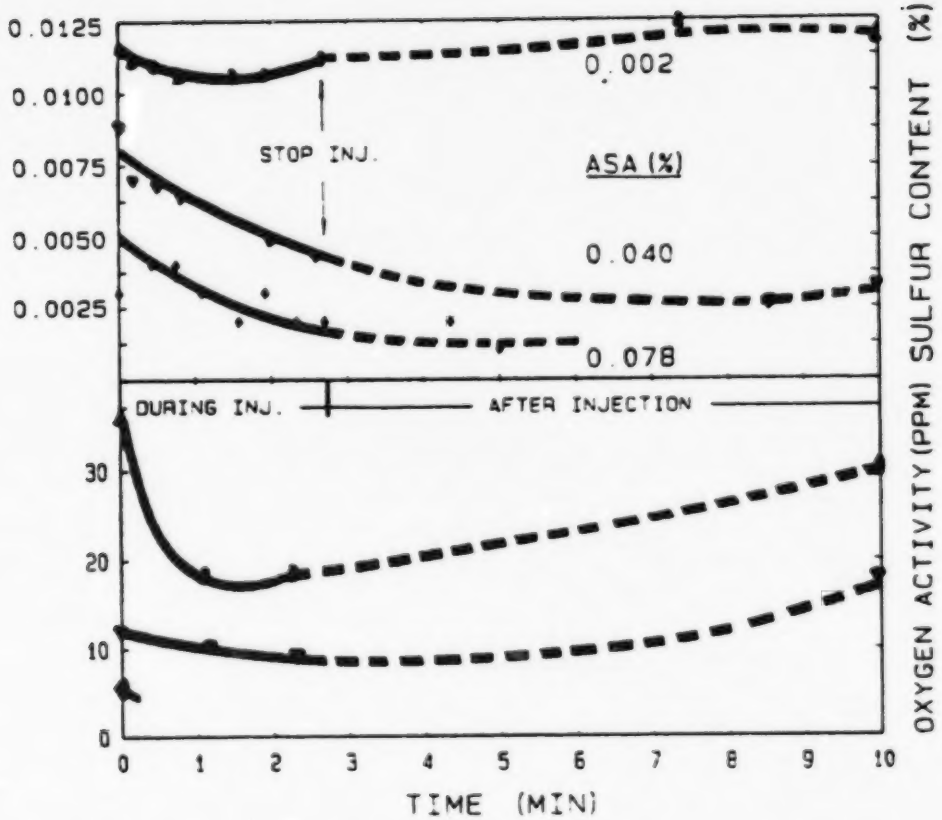

Figure 25: The effect of the acid soluble aluminum content of the steel on the changes in sulphur content (TOP) and oxygen activity (BOTTOM).

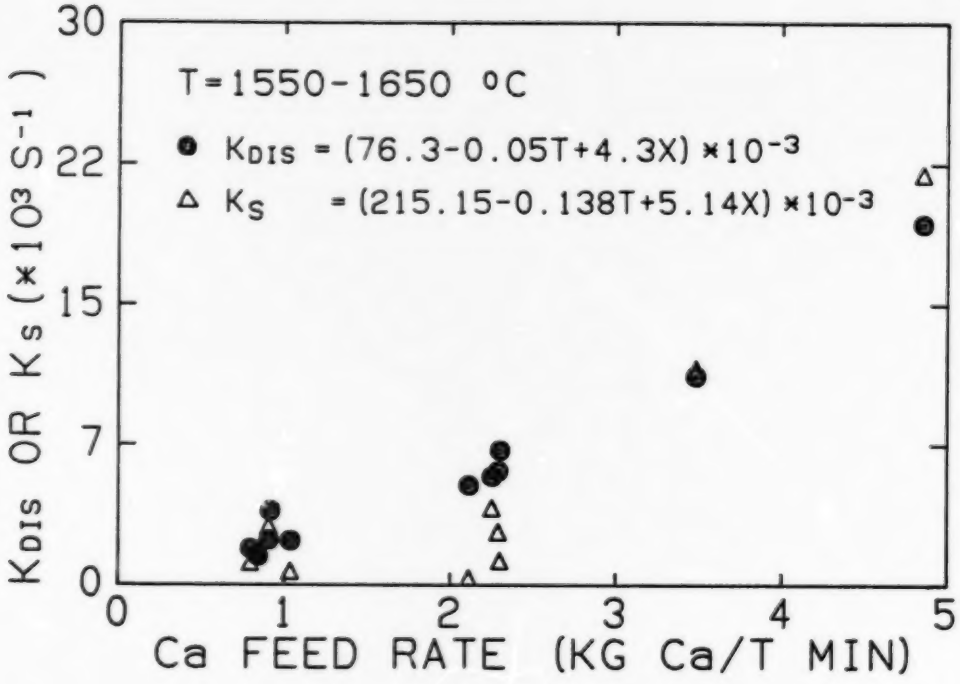

Figure 26: **The apparent first order rate constant for desulphurization, K_S as a function of calcium feed rate. The data is very similar to the rate constant for calcium pick-up, K_{DIS}. The equations represent regressions on the most important variables, the feed rate, X, and the temperature, T.**

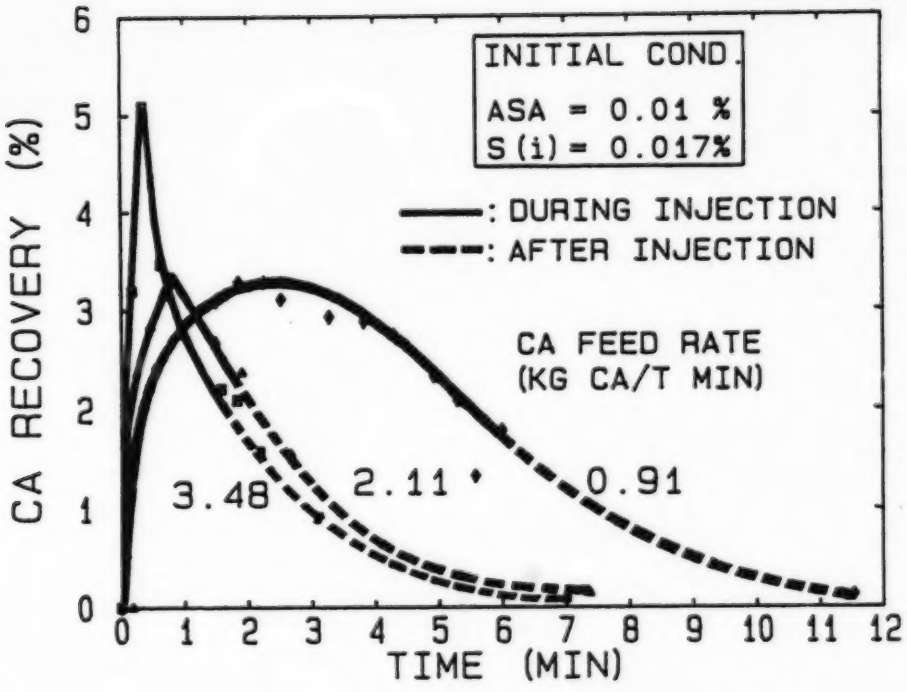

Figure 27: The calcium recovery as a function of time for three different injection rates.

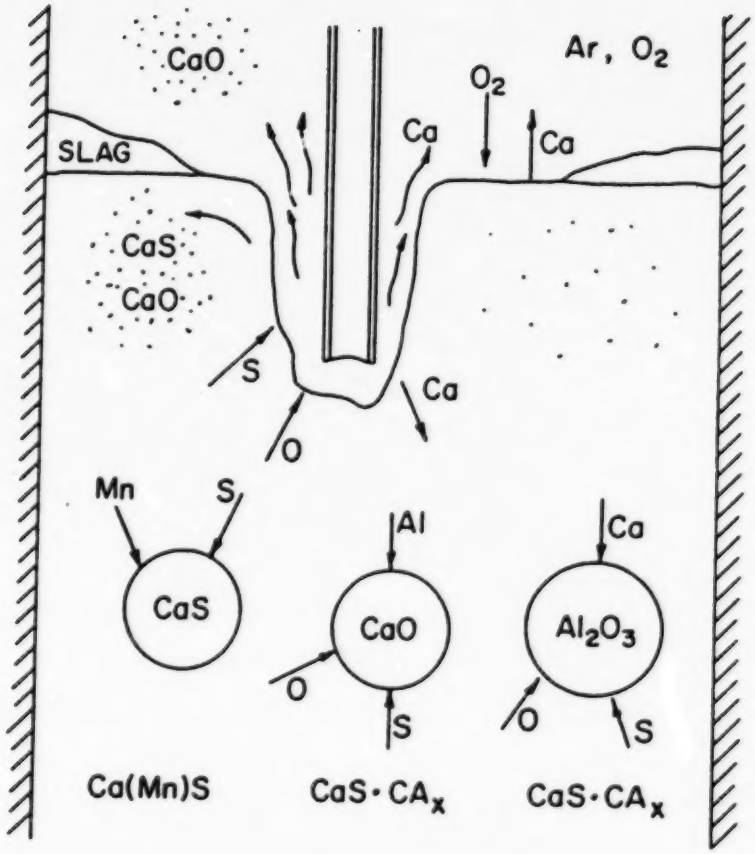

Figure 28: A schematic representation of the proposed model to explain the present experimental results.